Pearl and mushroom instability patterns in two miscible fluids' core annular flows

M. d'Olce, J. Martin, N. Rakotomalala, D. Salin, and L. Talon[a)]

Université Pierre et Marie Curie-Paris 6, Université Paris-Sud, CNRS, F-91405. Lab FAST, Bat 502, Campus Univ, Orsay, F-91405, France

We report on experiments with two miscible fluids of equal density but different viscosities. The fluids were injected co-currently and concentrically into a cylindrical pipe. The resulting base state is an axisymmetric parallel flow. The ratio of the two fluid flow rates determines the relative amount of the fluids, thus the radius of the inner core fluid. Depending on this radius and the total flow rate, two different and unstable axisymmetric patterns, denoted by mushrooms and pearls, were observed. We delineate the diagram of occurrence of the two patterns as a function of the various parameters. © *2008 American Institute of Physics*. [DOI: 10.1063/1.2838582]

I. INTRODUCTION

The hydrodynamic stability of two phase flows in a pipe has been widely investigated, both theoretically and experimentally,[1–7] following the pioneering theoretical work of Hickox.[8]

Miscible fluid displacement in the same geometry, in which an injected fluid displaces another initially occupying the pipe, has been addressed more recently, experimentally[9–13] and using numerical simulations.[14,15] When the displacing fluid is less viscous than the displaced one, a moving finger of the injected fluid develops and propagates into the fluid in place following a stationary profile, analogous to the Taylor's bubble observed in immiscible fluids.[16] Many studies have focused on the thickness of the displaced fluid layer left behind the finger, while some others have reported on the destabilization of the (pseudo-) interface between the fluids at large Reynolds numbers. Various patterns, such as axisymmetric sausagelike, or asymmetric corkscrew patterns have been reported.[10,13,17] Scoffoni *et al.*[13] delineated the stability map in the case of a stabilizing density contrast in such flows. They noticed that the observed instability was likely due to the destabilization of the quasiparallel flow upstream of the finger tip, as typically observed in immiscible core annular parallel flows.[2,5,18] Charru and Hinch[19] discussed the different mechanisms able to destabilize stratified parallel flows in plane Couette geometry, in the absence of surface tension and showed that the destabilization could result either from the ratio or the difference of the shear stress on both sides of the interface.

A recent numerical study[20] addressed the linear destabilization of miscible neutrally buoyant core annular parallel flows; such flows could exhibit corkscrew or axisymmetric unstable modes when the diffusion coefficient of mass and momentum are close to each other (Schmidt number close to unity therefore corresponding to gas flows). The study also indicates that at larger Schmidt numbers, the axisymmetric mode should prevail, and be observed for rather small Reynolds numbers and large wave numbers. These last predictions partly agree with the observation of corkscrew instabilities by Cao *et al.*,[21] at low Reynolds number, but using non-Newtonian power-law fluids. Here we report on experimental investigations of the nonlinear regime of unstable miscible Newtonian liquid core annular flows. For a fixed viscosity ratio (i.e., a fixed shear ratio at the interface), we delineate the occurrence of the different patterns, for varied Reynolds numbers and core fluid radius.

II. EXPERIMENTS

Experiments were performed in a vertical transparent Perspex cylindrical tube of 1 m length and an internal radius of $R=1.0$ cm. An upwards injection of the two fluids was implemented, using a concentric inner tube of radius smaller than R, as sketched in Fig. 1. Obtaining a parallel flow along the length of the tube required a sufficiently large inner tube radius (of internal and external radii equal to 0.75 cm and 0.85 cm, respectively). The core fluid and the wall fluid were simultaneously injected with two pumps, at the constant flow rates, Q_{core} and Q_{wall}, respectively. The apparatus was enclosed in a square box filled with water in order to avoid significant optical distortion, and a video camera recorded the fluid displacement. The optical contrast between the two fluids was obtained by blue dying of the core fluid. The use of a thin laser sheet (1 mm wide), illuminating a plane containing the central axis of the tube, allowed us to capture the details of the patterns in the plane (the dye was fluorescein in that case). Most of the experiments were conducted with water-natrosol mixtures, which can provide large variations in viscosity (typically from 10^{-3} to 0.3 Pa s), with small variations in density. These mixtures are perfectly Newtonian in the range of shear rates used in our experiments.[22,23] The core fluid viscosity and the viscosity ratio were chosen equal to $\eta_{core}=10^{-3}$ Pa s and $M=\eta_{wall}/\eta_{core}=25$, respectively. The fluid densities were matched to $\rho=999.8$ kg/m³ by adding calcium chloride. This leads to the following kinematic viscosities, $\nu_{core}=\eta_{core}/\rho=10^{-6}$ m²/s and $\nu_{wall}=25\times10^{-6}$ m²/s.

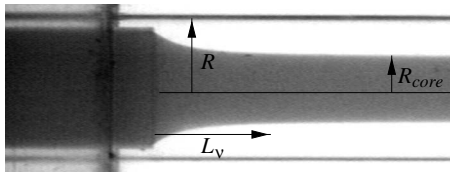a)Electronic mail: talon@fast.u-psud.fr.

20, 024104-1

FIG. 1. Sketch of the injection device used to implement core annular flow. The cylindrical tube (of 1 m length and $R=1.0$ cm radius) surrounds a concentric smaller tube (of inner radius 0.75 cm). The core fluid is injected into the smaller tube and the wall fluid is injected into the annular volume surrounding the small tube. The core flow converges towards a parallel flow over a viscous entry length, L_v.

For a given viscosity ratio, the experimental control parameters are the two fluid flow rates. The total flow rate, $Q=Q_{core}+Q_{wall}$, sets the average flow velocity, $\bar{U}=Q/(\pi R^2)$, and consequently the Reynolds and Péclet numbers of the experiment, $\mathrm{Re}=\bar{U}R/\nu_{core}$ and $\mathrm{Pe}=\bar{U}R/D_m$. The molecular diffusion coefficient, D_m, was estimated as in Refs. 22 and 23 to $D_m \simeq 10^{-10}$ m²/s, setting the Schmidt number to $\mathrm{Sc}=\nu/D_m \simeq 10^4$. The range of Re used in the experiment is between 2 and 60; the corresponding Pe ranged between 2×10^4 and 6×10^5. Parallel flow of the two fluids is established beyond a viscous inlet length, $L_v \simeq \bar{U}R^2/\nu_{core}$, which is of the order of 1 cm for the typical parameter values (Fig. 1). Under parallel flow conditions, the flow rates set the radius R_{core} of the core fluid. Assuming that the two fluids have not diffused (large Pe), the Poiseuille-type velocity profile expresses itself in terms of the relative core fluid radius $r=R_{core}/R$ as $v_1(h)=2\bar{U}[1-Mh^2+(M-1)r^2]/[1+(M-1)r^4]$ and $v_2(h)=2\bar{U}(1-h^2)/[1+(M-1)r^4]$ for $0<h<r$ and $r<h<1$, respectively (where h is the relative distance from the axis). This velocity profile is in reasonable agreement with our Particle Image Velocimetry (PIV) measurements beyond the viscous entry length. Accordingly, the relative core fluid radius satisfies the relation

$$\frac{Q_{core}}{Q}=\frac{2r^2+(M-2)r^4}{1+(M-1)r^4}. \tag{1}$$

As the above function is monotonic for $r \in [0,1]$, the relative core radius is uniquely determined from the flow ratio Q_{core}/Q. Moreover, the difference between the shears on both sides of the interface $\Delta\dot{\gamma}=4r(M-1)\bar{U}/[1+(M-1)r^4]R$ is almost linear in r, for $r^4<1/3(M-1)$, i.e., $r<0.35$ for $M=25$, so that r can be also considered as a measure of the
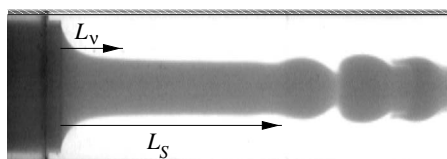

FIG. 2. Typical flow geometry near the injection plane. Depicted is the typical length, L_S, beyond which the parallel core flow destabilizes.
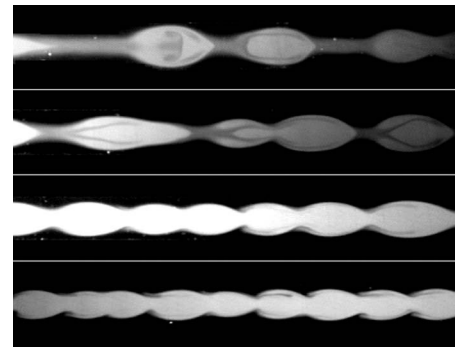

FIG. 3. Patterns observed at $r=0.25$ and for different values of Re increasing from top to bottom (Re=5,9,12,18). The sequence shows the evolution from a pearl-like to a mushroom-like pattern.

shear difference, $\Delta\dot{\gamma} \simeq 4r(M-1)\bar{U}/R$, in most of our experiments. In the following, the control of the relative flow rates will be expressed in terms of the variable r, for the sake of simplicity.

III. INSTABILITY PATTERNS

Figure 2 displays a typical flow geometry obtained in the vicinity of the tube inlet. We observe the following:

(a) Close to the injection, the convergence towards a parallel flow takes place over a viscous entry length, L_v, of the order of the tube radius R;

(b) Further downstream, the (pseudo-) interface between the fluids is parallel over a length L_s;

(c) Even further downstream, an instability pattern develops, the shape of which is "mushroom"- or "pearl"-like, depending on the values of Re and r.

Figure 3 shows instability patterns obtained for $r=0.25$ and different Re numbers (increasing from top to bottom in the figure). In the upper two panels, the instability results in a succession of "egg-shaped" patterns of the core fluid, denoted by pearl patterns; in the lower two panels, the patterns take the form of "mushrooms." They are closer to one an-
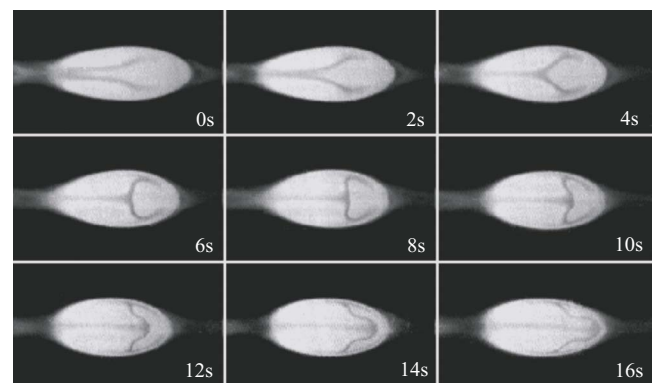

FIG. 4. (Color online) Time evolution of one particular pearl-like pattern, traveling at about 2 mm/s, at Re=10.5 and $r=0.26$. Time increases from left to right and from top to bottom. Notice the bursts of the wall fluid which propagate through the traveling pattern and exhibit a kind of umbrella inversion.
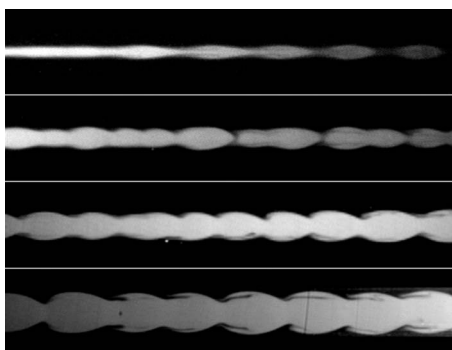
FIG. 5. Patterns observed at Re=18 and for different values of r increasing from top to bottom ($r=0.12,0.19,0.24,0.25$). The sequence shows the evolution from a pearl-like to a mushroom-like pattern.

FIG. 7. Normalized pattern wavelength, λ/R vs Re, for $r \simeq 0.26$ [($\bullet$): pearls, ($\blacktriangle$): mushrooms].

other and exhibit a curling backwards of the flow direction. Unlike the "mushrooms," the "pearls" are connected by thin filaments of diffuse core fluid. Figure 4 shows that the travelling "pearls" are crossed by bursts of the wall fluid swept along by the flow. These bursts exhibit a kind of "umbrella" inversion as they propagate through the "pearls."

Figure 5 shows instability patterns at Re=18 and different r values (increasing from top to bottom in the figure). Again, the patterns evolve from "pearls" to "mushrooms" as r increases.

The various patterns obtained for different values of Re and r are arranged in the $r-$Re plane of Fig. 6. The figure shows that mushroom patterns are obtained at large Re or large r, whereas pearl patterns correspond to smaller Re and r, and the boundary delineating the two corresponding regions is rather well defined. We note that for r larger than roughly 0.4 and for moderate values of Re, the fluid interface was too diffuse for the difference between the patterns to be discernible.

To characterize the patterns more quantitatively, we have measured their typical wavelengths, λ. Figure 7 plots the wavelength normalized by the tube radius R, as a function of Re, for $r \simeq 0.26$. For the mushroom patterns (larger Re) the wavelengths are of the order of R, and decrease when Re is
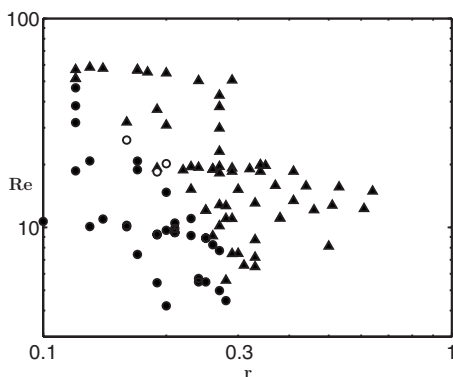
increased. This decrease holds, and may be even stronger, for the pearl patterns (below Re $\simeq 10$), and the wavelength is significantly larger than R. We note that this decrease over the range of Re is close to $\lambda \sim 1/\text{Re}^2$, which is not accounted for by any of the predictions of the linear stability analysis (either long wave or short wave regimes).[5,19]

IV. CONCLUSIONS

We report on core annular flow experiments with two neutrally buoyant miscible fluids of different viscosities. The radius of the less viscous core fluid was varied with the help of a centerline injector. Whatever the core fluid radius, the parallel flow obtained near the injection plane always destabilizes downstream, leading to two axisymmetric patterns the shape of which is either mushroom-like or pearl-like. The occurrence of these two patterns has been delineated; pearls form for small core radius or Reynolds number, and mushroom patterns are observed otherwise.

ACKNOWLEDGMENTS

FIG. 6. Domain of occurrence of the two patterns in the $r-$Re plane. Mushroom-like patterns ($\blacktriangle$) are obtained at large Re or r; pearl-like patterns ($\bullet$) correspond to smaller Re and r. The empty symbol ($\circ$) denotes the coexistence of the two patterns in the same experiment.

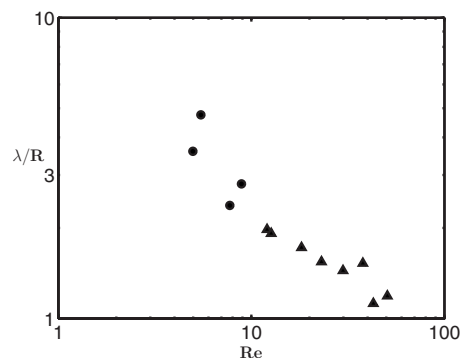[1] H. H. Hu and D. D. Joseph, "Lubricated pipelining: Stability of core-annular flow. Part 2," J. Fluid Mech. **205**, 395 (1989).

[2] D. D. Joseph, R. Bai, K. P. Chen, and Y. Y. Renardy, "Core-annular flows," Annu. Rev. Fluid Mech. **29**, 65 (1997).

[3] D. D. Joseph, M. Renardy, and Y. Renardy, "Instability of the flow of two immiscible liquids with different viscosities in a pipe," J. Fluid Mech. **141**, 309 (1984).

[4] D. D. Joseph and Y. Y. Renardy, *Fundamentals of Two-Fluid Dynamics. Part I: Mathematical Theory and Applications* (Springer-Verlag, New York, 1992).

[5] D. D. Joseph and Y. Y. Renardy, *Fundamentals of Two-Fluid Dynamics. Part II: Lubricated Transport, Drops and Miscible Liquids* (Springer-Verlag, New York, 1992).

[6] C. Kouris and J. Tsamopoulos, "Dynamics of axisymmetric core-annular flow in a straight tube. I. The more viscous fluid in the core, bamboo waves," Phys. Fluids **13**, 841 (2001).

[7] C. Kouris and J. Tsamopoulos, "Dynamics of the axisymmetric core-annular flow. II. The less viscous fluid in the core, saw tooth waves," Phys. Fluids **14**, 1011 (2002).

[8] C. E. Hickox, "Instability due to viscosity and density stratification in axisymmetric pipe flow," Phys. Fluids **14**, 251 (1971).

[9] R. Balasubramaniam, N. Rashidnia, T. Maxworthy, and J. Kuang, "Instability of miscible interfaces in a cylindrical tube," Phys. Fluids **17**, 052103 (2005).

[10] C. Gabard and J.-P. Hulin, "Miscible displacement of non-Newtonian fluids in a vertical tube," Eur. Phys. J. E **11**, 231 (2003).

[11] E. Lajeunesse, J. Martin, N. Rakotomalala, D. Salin, and Y. C. Yortsos, "Miscible displacement in a Hele-Shaw cell at high rates," J. Fluid Mech. **398**, 299 (1999).

[12] P. Petitjeans and T. Maxworthy, "Miscible displacements in capillary tubes. Part 1. Experiments," J. Fluid Mech. **326**, 37 (1996).

[13] J. Scoffoni, E. Lajeunesse, and G. M. Homsy, "Interface instabilities during displacement of two miscible fluids in a vertical pipe," Phys. Fluids **13**, 553 (2001).

[14] C.-Y. Chen and E. Meiburg, "Miscible displacement in capillary tubes. Part 2. Numerical simulations," J. Fluid Mech. **326**, 57 (1996).

[15] N. Rakotomalala, D. Salin, and P. Watzky, "Miscible displacement between two parallel plates: BGK lattice gas simulations," J. Fluid Mech. **338**, 277 (1997).

[16] G. I. Taylor, "Deposition of a viscous fluid on the wall of a tube," J. Fluid Mech. **10**, 161 (1961).

[17] E. Lajeunesse, J. Martin, N. Rakotomalala, and D. Salin, "3D instability of miscible displacements in a Hele-Shaw cell," Phys. Rev. Lett. **79**, 5254 (1997).

[18] R. Bai, K. Chen, and D. D. Joseph, "Lubricated pipelining: stability of core-annular flow. Part 5. Experiments and comparison with theory," J. Fluid Mech. **240**, 97 (1992).

[19] F. Charru and E. J. Hinch, "'Phase diagram' of interfacial instabilities in a two-layer Couette flow and mechanism for the long-wave instability," J. Fluid Mech. **414**, 195 (2000).

[20] B. Selvam, S. Merk, R. Govindarajan, and E. Meiburg, "Stability of miscible core-annular flows with viscosity stratification," J. Fluid Mech. **592**, 23 (2007).

[21] Q. Cao, A. L. Ventresca, K. R. Sreenivas, and A. K. Prasad, "Instability due to viscosity stratification downstream of a centerline injector," Can. J. Chem. **81**, 913 (2003).

[22] M. Le Bars and A. Davaille, "Stability of thermal convection in two superimposed miscible viscous fluids," J. Fluid Mech. **471**, 339 (2002).

[23] R. S. Torrest, "Rheological properties of aqueous solutions of the polymer natrosol 250 hhr," J. Rheol. **26**, 143 (1982).